Hydraulic jumps & the role of surface tension

Physics Letters A 451 (2022) 128418

Contents lists available at ScienceDirect

Physics Letters A

www.elsevier.com/locate/pla

Hydraulic jumps & the role of surface tension

Edward Calver [a], Tristan Pryer [a], Alex V. Lukyanov [b,*]

[a] Department of Mathematical Sciences, University of Bath, Bath, BA2 7AY, UK
[b] School of Mathematical and Physical Sciences, University of Reading, Reading, RG6 6AX, UK

ARTICLE INFO

Article history:
Received 12 May 2022
Received in revised form 10 August 2022
Accepted 1 September 2022
Available online 6 September 2022
Communicated by A. Das

Keywords:
Hydraulic jumps
Surface tension
Regular solutions

ABSTRACT

Recent experiments involving generation of a hydraulic jump in liquid flows have led to a number of disputes about the role of surface tension in the process. This in turn instigated a revision of the main mechanisms and criteria of the jump formation. To clarify the issue of the surface tension effects, we have analysed liquid flows with a hydraulic jump region in the framework of a full depth-averaged thin film model (DAM). After benchmarking the model, we have performed broad parametric analysis of the problem. It has been established that while there is excellent agreement with the laminar flow observations, the surface tension effects only contribute to the shape of the transition region, but do not affect the position of the jump, that is, they are practically negligible. The results have repercussions on further developments of the jump formation theory, in particular, on the role of turbulence effects.

1. Introduction

The phenomenon of a hydraulic jump, which is commonly observed in free surface flows, is well known to the research community. However, despite of almost a century of intensive research [1–31], the phenomenon itself and its mechanisms are still the subject of hot debates [21–31].

In general, hydraulic jumps could be of many different forms [14,16], but the most studied are circular jumps, which are commonly observed in jet flows impinging on solid walls, and planar hydraulic jumps, which are usually observed in channel flows [8,12,16,21,26].

Recent debates have been instigated by new experimental evidence indicating that the position of a hydraulic jump is practically independent of the gravity field direction to the substrate where the flow with a jump takes place [17,18,20–22]. That is when a liquid jet of certain intensity impinges on solid walls oriented at different angles to the gravity force, the hydraulic jump radius measures almost the same at a fixed value of the total liquid flux in the jet.

These observations in line with the previously reported data obtained in low gravity conditions [10,13] inspired a revision of the main mechanisms involved in the jump formation, emphasising the role of the surface tension, and the subsequent polemic [21–25,27,29].

Indeed, the role of gravity in the formation of a hydraulic jump is well known. Continuity of mass and momentum fluxes across the jump region treated as a discontinuity implies on average that at that point

$$\frac{Y(1+Y)}{2Fr^2} + \frac{h_U}{R_0} Y We^{-1} = 1, \tag{1}$$

which can be used to estimate the position of the jump and its magnitude if somehow the free surface profiles are provided [11,15]. Here $Y = \frac{h_D}{h_U}$ is the ratio of the interface height h_D in the downstream region, straight after the jump, to that in the upstream region h_U, just before the jump, R_0 is the jump radius, $Fr^2 = \frac{6}{5}\frac{q_0^2}{g_0 h_U^3}$ and $We = \frac{6}{5}\frac{\rho q_0^2}{\gamma h_U}$ are the local values of the Froude and Weber numbers defined through the upstream height h_U, q_0 is the volumetric flux density per the unit length of the jump, γ is surface tension and g_0 is the acceleration of gravity.

As the aspect ratio of the layer height to the jump radius R_0 (in the case of a circular jump geometry), $\frac{h_U}{R_0} \ll 1$, is usually very small or zero in the case of a planar jump, contribution of the surface tension could be neglected leading to the classical Bélanger equation [32]

$$Y = \frac{\sqrt{1+8Fr^2} - 1}{2}. \tag{2}$$

In a simplified approach, the position of the jump can be roughly estimated as the critical point of the average velocity gradient [15] leading to a local condition

* Corresponding author.
E-mail address: a.lukyanov@reading.ac.uk (A.V. Lukyanov).

https://doi.org/10.1016/j.physleta.2022.128418

$$Fr = 1. \tag{3}$$

Criterion (3) is approximate and can not in principle distinguish different far-field conditions, as it was rightly noticed in [25], while the far-field can dramatically affect the flow and the development of a hydraulic jump [15].

Both conditions (2) and (3) imply that the main mechanism of the hydraulic jump formation is supposed to be due to gravity. Somehow, the opposite was observed in recent experiments [17,18,20–22].

Based on the experimental observations [17,18,20–22], the local condition (3) was revisited and modified to [21,22]

$$We^{-1} + Fr^{-2} = 1, \tag{4}$$

which is supposed to be fulfilled in the case of an arbitrary jump geometry.

The modified criterion (4) is still local and lacks information from the downstream conditions. But, it mitigates the effect of gravity while amplifying the role of the surface tension. As a result, other (different) trends are expected with the change of the controlling parameters of the flow (such as the total flux) and the liquid properties (such as surface tension) [22]. Condition (4) has been the subject of a polemic in the subsequent publications [23–31].

The authors of [23], using the full system of the Navier-Stokes equations, though in simplifying assumptions of laminar flow conditions, have concluded that there are possibly two typical scenarios, capillary-dominant and gravity-dominant regimes.

On the other hand, the authors of [24], also using the full Navier-Stokes model in the laminar flow regime, have come to a conclusion that gravity still plays the dominant role, but the flow becomes oscillatory unstable, when the coefficient of surface tension exceeds some critical value, which turned out to be well below the real values of the surface tension for such liquids as water. So that, the surface tension was found to be a destabilising factor in numerical simulations.

At the same time, in a recent study [29], the authors have demonstrated that there is compelling experimental evidence to doubt that the role of the surface tension is negligible, and the gravity dominates in the observed effects, as it would follow from (2) and (3).

One can summarise that at the moment the opinions are polarised about the contribution of surface tension and gravity effects to the process of the jump formation. Moreover, no air-tight explanation for the effect of the invariance to the gravity force direction has been proposed. The role of the surface tension, as a destabilising factor, also requires some further clarification to understand the extent that this mechanism can affect the formation of the transition region between the two separated zones, the upstream and the downstream regions. One needs to note that similar oscillatory behaviour has been reported in numerical simulations [26], while in their experimental observations such a feature was not clearly presented or identified.

The purpose of the current study is to clarify the role of the surface tension in the formation of a hydraulic jump. To eliminate all doubts about the surface tension contribution, we concentrate on the analysis of a generic case with a planar hydraulic jump in laminar conditions, such that any overshadowing effects of turbulence [3,16,20] can be safely ruled out.

The generation of a hydraulic jump is analysed theoretically using an advanced numerical scheme and a depth-averaged model (DAM), which is widely accepted as a reasonable approximation in many practical applications in the absence of turbulence effects. One needs to note here that all aforementioned criteria (2), (3) or (4), widely used in interpretation of experimental data in various conditions, have been obtained using in fact the same layer averaging as that used in the derivation of the full DAM.

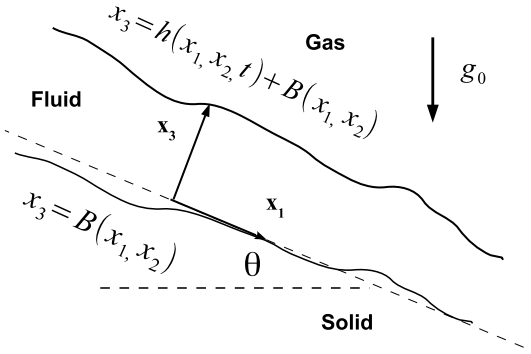

Fig. 1. Illustration of the thin film flow geometry.

The advantage of this practical approach in comparison to the full system of the Navier-Stokes equations is its computational efficiency in view of Courant-Friedrichs-Lewy stability restrictions. Applications of more detailed models, which might be more general in terms of the parameter range, are always hindered by the high computational costs. In that case, the spatial resolution is bound to be rather limited, leading to as a consequence to either focusing on simulations in strictly laminar conditions or to numerical artifacts associated with small scale vortex motion, which are obviously absent in the applications of the DAMs.

As we will demonstrate further, even in simple geometries, high spatial resolution is required to adequately describe the transition region if surface tension effects are to be included in full.

In contrast to the common trend [23,24], when the DAM is used neglecting high order terms, associated with surface tension effects, to obtain analytical though discontinuous solutions, we employ the full DAM, which is supposed to have continuous solutions throughout the transition region. This should be sufficient to establish the role played by surface tension without any doubts. We demonstrate, by comparison with experiments, that the DAMs can always provide a regular weak solution continuously linking the two regions of the flow, which carries, in fact, all the features available in the more detailed models or approximations, including the effects of surface tension.

In what follows, we first briefly provide a mathematical model relevant to the DAM approximation and revisit previous analytical results mostly involving discontinuous solutions, and then turn our attention to continuous solutions relevant to laminar flow regimes and parametric dependencies, including the effects of surface tension.

2. The mathematical model

The utilised mathematical model is relatively well understood, so that details can be found elsewhere [33]. This is a three-dimensional viscous flow of a Newtonian liquid at a solid wall located at $x_3 = B(x_1, x_2)$ with a free surface parametrised accordingly $x_3 = h(x_1, x_2, t) + B(x_1, x_2)$, Fig. 1.

The problem is characterised by two different length scales H and L in the vertical, x_3, and the horizontal x_1, x_2 directions respectively. Angle θ characterises the inclination of the flow plane to the direction of the gravity field $\mathbf{g_0}$, Fig. 1. In the thin film approximation taken in the study $H/L = \delta \ll 1$ is assumed to be a small parameter.

The non-dimensional formulation is achieved by introducing reduced variables, that is the coordinates $x_1 = \hat{x}_1/L$, $x_2 = \hat{x}_2/L$, $x_3 = \hat{x}_3/H$, velocities $v_1 = \hat{v}_1/U$, $v_2 = \hat{v}_2/U$, $v_3 = \hat{v}_3/\delta U$, time t/t_0 and pressure $p = \hat{p}/p_0$. Here U is characteristic velocity, $t_0 = L/U$

is the timescale, $p_0 = \rho U^2$ is the characteristic pressure in the inertial range, ρ is the liquid density.

The system of the governing equations in the thin film approximation is obtained by introducing averaged (over the layer) quantities

$$q_{1,2} = \int_B^{h+B} v_{1,2}\, dx_3.$$

As a result of the averaging procedure

$$\frac{\partial h}{\partial t} + \frac{\partial q_1}{\partial x_1} + \frac{\partial q_2}{\partial x_2} = 0, \tag{5}$$

$$\frac{\partial q_1}{\partial t} + \frac{6}{5}\frac{\partial}{\partial x_1}\left(\frac{q_1^2}{h}\right) + \frac{6}{5}\frac{\partial}{\partial x_2}\left(\frac{q_1 q_2}{h}\right) = h\left\{Ka_{\parallel}\sin\theta - \frac{\partial p}{\partial x_1}\right\} - \frac{3}{Re}\frac{q_1}{h^2} \tag{6}$$

and

$$\frac{\partial q_2}{\partial t} + \frac{6}{5}\frac{\partial}{\partial x_1}\left(\frac{q_1 q_2}{h}\right) + \frac{6}{5}\frac{\partial}{\partial x_2}\left(\frac{q_2^2}{h}\right) = -h\frac{\partial p}{\partial x_2} - \frac{3}{Re}\frac{q_2}{h^2}, \tag{7}$$

where pressure p is given in the hydrostatic approximation by

$$p = p_a + Ka\cos\theta\,(h + B - x_3) - \frac{1}{\hat{Ca}\,Re}\left(\frac{\partial^2(h+B)}{\partial x_1^2} + \frac{\partial^2(h+B)}{\partial x_2^2}\right). \tag{8}$$

Here p_a is external gas pressure. The non-dimensional parameters of the problem are the Reynolds number, $Re = \delta\frac{\rho U H}{\mu}$, the Kapitza numbers, $Ka_{\parallel} = \frac{g_0 L}{U^2}$ and $Ka = \frac{g_0 H}{U^2}$ and $\hat{Ca} = Ca\,\delta^{-3}$, which is a renormalised Capillary number $Ca = \frac{\mu U}{\gamma}$, where γ and μ are surface tension and dynamic viscosity of the liquid respectively.

To understand the functionality of the thin film system of equations (5)-(8) and the admissible solutions, we further simplify the problem to a one-dimensional case on a flat substrate, $B = 0$, when a planar hydraulic jump is regularly observed.

2.1. One-dimensional steady state problem

On a flat substrate, $B = 0$, and in a one-dimensional Cartesian case

$$\frac{\partial h}{\partial t} + \frac{\partial q}{\partial x} = 0, \tag{9}$$

$$\frac{\partial q}{\partial t} + \frac{6}{5}\frac{\partial}{\partial x}\left(\frac{q^2}{h}\right) = -\frac{3}{Re}\frac{q}{h^2} - h\left(Ka\cos\theta\,\frac{\partial h}{\partial x} - Ka_{\parallel}\sin\theta - \frac{1}{\hat{Ca}Re}\frac{\partial^3 h}{\partial x^3}\right). \tag{10}$$

In a steady state $q = const$, and

$$0 = \frac{h^3}{\hat{Ca}Re}\frac{\partial^3 h}{\partial x^3} + \frac{\partial h}{\partial x}\left(\frac{6}{5}q^2 - Ka\cos\theta h^3\right) + h^3\,Ka_{\parallel}\sin\theta - \frac{3q}{Re}. \tag{11}$$

There are, in general, four non-dimensional parameters in the model reflecting the roles of gravity (Ka and $Ka_{\parallel}$), surface tension ($\hat{Ca}$), viscosity and inertia (Re). The non-dimensional parameter Ka is actually the inverse Froude number $Fr^2 = \frac{6}{5}Ka^{-1}$.

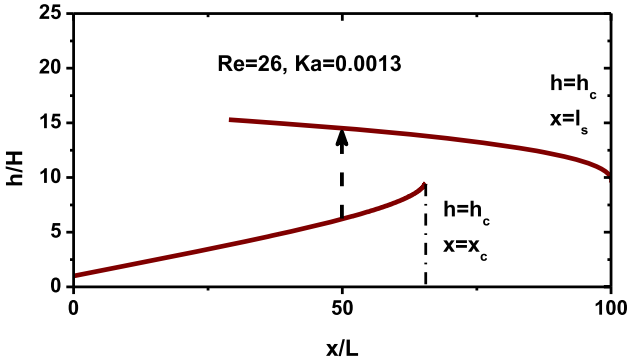

Fig. 2. Illustration of the two branches of the steady state solutions, (13) and (16), at $Re = 26$, $Ka = 0.0013$, $\hat{Ca} = 108$ and $l_s = 100$. The arrow is the jump position according to (2).

2.2. Hydraulic jump as a discontinuity

If $\hat{Ca}Re \gg 1$ (as in many experiments), the higher order term in (11), which is solely due to surface tension, can be formally neglected. This widely-used approximation in the case $\theta = 0$, when the gravity is perpendicular to the liquid layer, leads to

$$\frac{\partial h}{\partial x}\left\{\frac{6}{5}q^2 - Ka\,h^3\right\} = \frac{3q}{Re} \tag{12}$$

which has discontinuous solutions.

Solving equation (12) with $h(0) = 1$ and $q = 1$ (if one chooses $H = h_0$), one gets

$$\frac{6}{5}(h-1) - \frac{Ka}{4}(h^4 - 1) = \frac{3}{Re}x. \tag{13}$$

The obtained solution has a critical point at

$$h_c^3 = \frac{6}{5\,Ka} \tag{14}$$

and covers the range

$$x \le x_c = \frac{6}{5}(h_c - 1) - \frac{Ka}{4}(h_c^4 - 1).$$

This is the upstream branch, see Fig. 2.

The second solution, the downstream branch, Fig. 2, can be obtained from the far-field condition at $x = l_s$ in a similar way as in [15,16] by placing the critical point at $x = l_s$, that is

$$h = h_c, \quad x = l_s. \tag{15}$$

Boundary condition (15) mimics overflow at the end of the substrate. The downstream profile then is described by

$$\frac{6}{5}(h - h_c) - \frac{Ka}{4}(h^4 - h_c^4) = \frac{3}{Re}(x - l_s). \tag{16}$$

The obtained discontinuous solution cannot connect the upstream region to the downstream far-field. The discontinuity is inherent to this approximation due to the low order of the differential equation with a critical point. Neither the approximate solution can describe the shape of the jump itself and inform us about the position of the jump, which may occur anywhere $x < x_c$, subject to an additional condition of the mass and momentum flux continuity [11,15].

In what follows, we consider the full DAM including the higher order term to obtain continuous solutions and analyse the effects of the surface tension. The results, obtained numerically, are compared with the experimental profiles observed in laminar flow conditions serving to provide a benchmark case and inform us

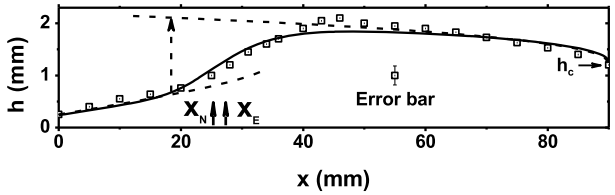

Fig. 3. Illustration of the experimental free surface profile (symbols) in a laminar regime from [26] at $\theta = 0°$, $q_0 = 1.25 \cdot 10^{-4}\,\mathrm{m}^2/\mathrm{s}$, $Re = 12.5$, $\hat{Ca} = 6.9$ and $Ka = 0.0098$. The dashed lines are analytical solutions (13) and (16), the solid line is the numerical solution of (9) - (10) after reaching a steady state. The vertical arrows are the positions of the inflection points of the experimental and numerical profiles, X_E and X_N, respectively, and the jump according to (2). The dimensional parameters $h_0 = 0.25\,\mathrm{mm}$ and $l_s = 90\,\mathrm{mm}$.

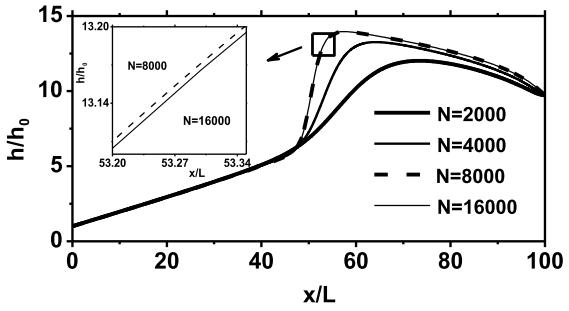

Fig. 4. Free surface profiles calculated numerically at $\theta = 0°$, $Re = 26$, $\hat{Ca} = 108$ and $Ka = 0.0013$ and at different spatial resolutions $\Delta x = 100/N$, where N is the number of intervals.

about the accuracy of the approach. Then the model is used to analyse parametric dependencies. We will focus on recent experimental observations [26].

3. Continuous solutions and experiment in laminar flow regimes

The main, input and output, dimensional parameters of the flows with a jump are the volumetric flux density q_0, the initial film thickness h_0 at the entrance of the flow and the position of the jump X with respect to the entry point. The jump position is defined in this study as the inflection point of the continuous free surface profiles.

The formation of a planar hydraulic jump in a laminar flow regime has been recently studied in detail with free surface profiles observed at different inclination angles $-0.6° \le \theta \le 1.5°$ [26].

The dimensional volumetric flux density in the experiments q_0 spans

$$5 \cdot 10^{-5}\,\mathrm{m}^2\,\mathrm{s}^{-1} \le q_0 \le 2 \cdot 10^{-4}\,\mathrm{m}^2\,\mathrm{s}^{-1},$$

while $h_0 = 0.25\,\mathrm{mm}$.

Accordingly, the range of the non-dimensional parameters of the problem based on the upstream conditions and water as the experimental liquid then suggest, $5 \le Re \le 20$, $3 \le \hat{Ca} \le 11$ and $4 \cdot 10^{-3} \le Ka \le 6 \cdot 10^{-2}$, if we define $H = h_0$, the characteristic velocity by means of $q_0 = Uh_0$, so that non-dimensional quantity $q = 1$. The horizontal length scale L is chosen on the basis of h_0 by setting $\delta = 0.1$, so that $4 \cdot 10^{-2} \le Ka_{\parallel} \le 6 \cdot 10^{-1}$. This choice of the parameter δ corresponds to the minimal horizontal length scale of the free surface variations observed.

In a particular case of $\theta = 0°$, the profile is demonstrated in Fig. 3, where the branches of the analytical solutions (13) and (16) are shown for comparison. The analytical solutions were generated using the far field condition (15) at the channel end at $l_s = 90\,\mathrm{mm}$ (non-dimensional channel length $l_s = 36$) and the initial film thickness $h_0 = 0.25\,\mathrm{mm}$ (non-dimensional $h(0) = 1$) at $x = 0$ at the flow inlet. The use of the overflow condition is justified as, according to (14), $h_c = 1.24\,\mathrm{mm}$, while the last experimental point at the substrate end is at $h(l_s) = 1.2 \pm 0.2\,\mathrm{mm}$.

As one can observe, the solutions match the experimental profile very well away from the jump region. In particular, one can see the typical linear dependence in the upstream part as is expected from (13). The location of the hydraulic jump according to (2) is practically at the point where the experimental profile starts to deviate from the upstream branch of the solution, which is shown by the dashed arrow in the figure. The subsequent values of the local non-dimensional parameters at that point are $Fr^2 \approx 7$ and $We \approx 0.4$ ($1 < Fr^2 < 120$, $0.2 < We < 1$, $0 < x < x_c$), so that neither (3) nor (4) are fulfilled at that point or further downstream at the inflection point.

Consider now numerical solutions of the DAM (9)-(10). The third order partial differential equation has sufficient degrees of freedom to satisfy boundary conditions at the inlet and the outlet of the flow. Problem (9)-(10) is solved numerically with two boundary conditions at each end of the interval $x \in [0, l_s]$ to reach a steady state in time. That is,

$$h(0,t) = 1, \quad q(0,t) = 1 \tag{17}$$

at the inlet at $x = 0$, and

$$h(l_s,t) = h_c, \quad q(l_s,t) = 1 \tag{18}$$

at the outlet at $x = l_s$. The details of the numerical method can be found in Appendix.

To verify the method converges we fix parameters $Re = 26$, $\hat{Ca} = 108$, $Ka = 0.0013$ and simulate solutions over a family of mesh sizes until a steady state is achieved. The numerical profiles are shown in Fig. 4 at $\Delta x \in [0.00625, 0.05]$.

As one can readily observe, the requirements for minimal spatial resolution are quite demanding. In case the full Navier-Stokes model would be applied, this kind of refinement may be very computationally expensive. On the other hand, if the resolution is insufficient numerical artifacts may appear. To ensure physically accurate results, all our experiments henceforth were obtained using $\Delta x = 0.00625$.

In the comparison, we have numerically generated a profile observed at $\theta = 0°$ and $q_0 = 1.25 \cdot 10^{-4}\,\mathrm{m}^2/\mathrm{s}$, which corresponds to non-dimensional parameters $Re = 12.5$, $\hat{Ca} = 6.9$ and $Ka = 0.0098$, Fig. 3, using the boundary conditions (17)-(18) at the flow inlet, where $h(0,t) = 1$, and at the flow outlet at $x = l_s = 36$ corresponding to the dimensional channel length $l_s = 90\,\mathrm{mm}$.

Note that no adjustment of the parameters used for the simulations was involved in this case, while in some other cases (used for the comparison), where the mismatch between h_c and $h(l_s)$ (observed in the experiments) was larger, the actual value $h(l_s)$ was used instead of h_c in (18), as is demonstrated in Fig. 6.

As one can observe, Fig. 3, the numerical solution (which is a typical example) provides a very good approximation to the experimental dependence within the experimental error involved. It closely follows the asymptotic solution in the upstream region till the point where the jump starts developing. In the downstream region, the numerical solution follows the asymptotic solution straight after the maximum is achieved, as is expected.

Remarkably, the inflection points of the experimental and numerical profiles, X_E and X_N, corresponding to the midpoints of the jump region were found to be very close to each other.

In the second set of simulations in the comparison, we mimicked the change of the flow rate q_0 in the experiments at different inclination angles θ and followed the position of the jump using the same approach to the far field conditions.

The non-dimensional parameters were scaled from reference values $R^{(0)}$, $\hat{C}^{(0)}$, $Ka^{(0)}$ and $Ka_{\parallel}^{(0)}$ at different inclination angles

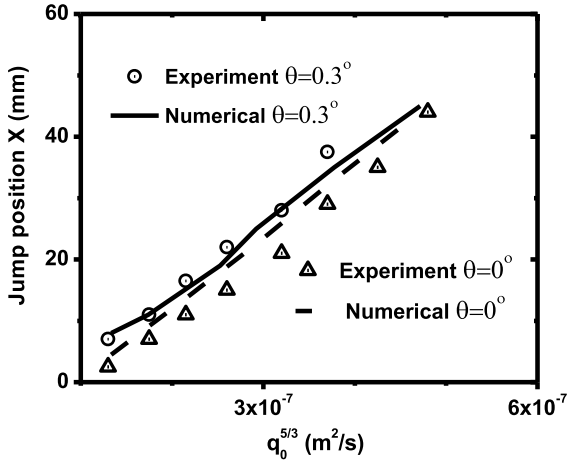

Fig. 5. Hydraulic jump position X as a function of the flow rate $q_0^{5/3}$ in the experiments [26] (symbols) and numerical simulations at $\theta = 0°$ (the dashed line) and at $\theta = 0.3°$ (the solid line). The dimensional parameters $h_0 = 0.25$ mm and $l_s = 90$ mm.

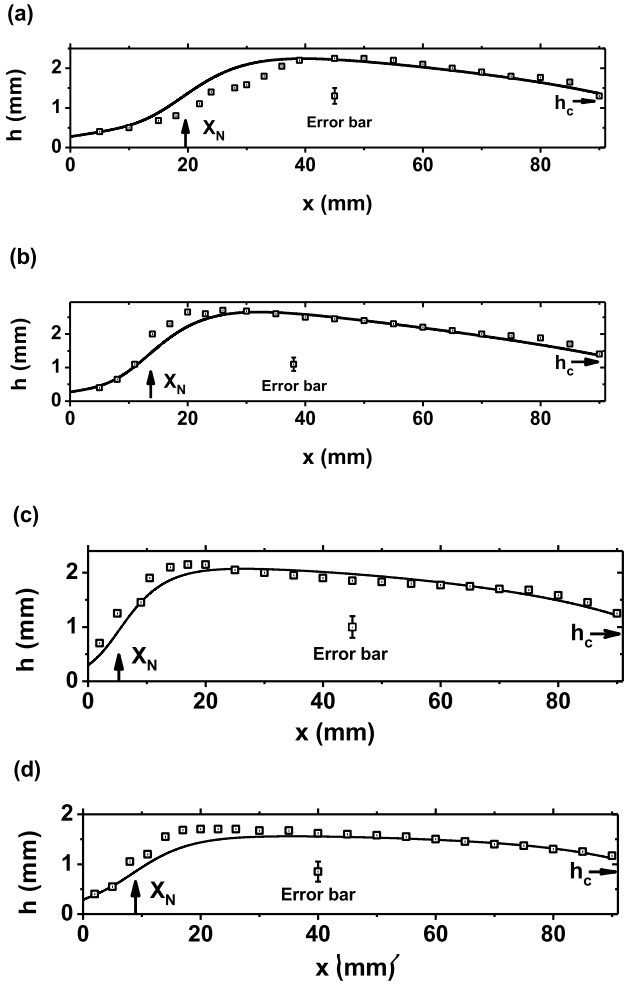

Fig. 6. (a) Illustration of the experimental free surface profile (symbols) in a laminar regime from [26] at $q_0 = 12.5 \cdot 10^{-5}$ m^2/s, $Re = 12.5$, $\hat{Ca} = 6.9$, $Ka = 0.0098$, $Ka_{\parallel} = 0.098$ and $\theta = -0.3°$. The solid line is the numerical solution of (9) - (10) after reaching a steady state with the far field condition set using observed values of $h(l_s)$. The arrow is the position of the inflection point of the numerical profile X_N. (b) Similar to part (a) but at $\theta = -0.6°$. (c) Similar to part (a) but at $q_0 = 7.5 \cdot 10^{-5}$ m^2/s, $Re = 7.5$, $\hat{Ca} = 4.14$, $Ka = 0.027$, $Ka_{\parallel} = 0.27$ and $\theta = 0°$. (d) Similar to part (c) but at $\theta = 0.3°$. The dimensional parameters $h_0 = 0.25$ mm and $l_s = 90$ mm.

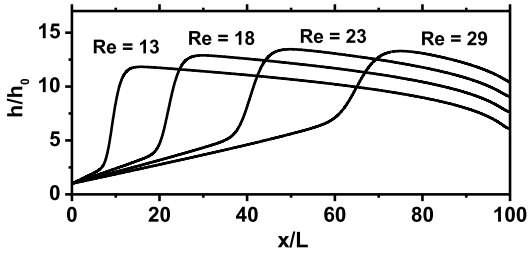

Fig. 7. Free surface profiles calculated numerically in the parameter range relevant to the experiments [16] at $\theta = 0°$. The non-dimensional parameters were scaled up and down from the reference values $Re^{(0)} = 26$, $\hat{Ca}^{(0)} = 108$ and $Ka^{(0)} = 1.3 \cdot 10^{-3}$ to mimic variations of the flux according to $Re = Sc\, Re^{(0)}$, $\hat{Ca} = Sc\, \hat{Ca}^{(0)}$ and $Ka = Ka^{(0)}/Sc^2$, where $0.5 \le Sc \le 1.1$.

according to $Re = Sc\, R^{(0)}$, $\hat{Ca} = Sc\, \hat{C}^{(0)}$, $Ka = Ka^{(0)}/Sc^2$ and $Ka = Ka_{\parallel}^{(0)}/Sc^2$ where Sc was the scaling factor.

One can observe the trend found in experiments that the jump position follows $X \propto q_0^{5/3}$, Fig. 5. Variations of the inclination angles in the numerical solutions also demonstrated the trends observed in the experiments, Figs. 5 and 6. The inflection point was moving closer to the inlet at the negative inclination angles (when the absolute value of θ increases) and in the opposite direction at the positive values of θ.

One can conclude that the full DAM provides adequate description of laminar flows generating regular solutions with smooth, continuous free surface profiles.

We note, even though the model parameters in the simulations were taken at real surface tension values for water, there was no transient oscillatory behaviour observed, but a steady-state. So, the transient features observed in the Navier-Stokes laminar flow simulations [24] were either averaged out in the DAM or could be computational artifacts of the numerical scheme due to insufficient spatial resolution. Note that possibly similar oscillatory features were observed in numerical simulations presented in [26], while, as one can see in Figs. 10 and 11 of [26], the experimental profiles demonstrated smoother variations.

4. Parametric dependencies of the full DAM

Consider now how variations of the main parameters of the system affect the flow and the formation of the jump transition region. As a reference point, for demonstration, we choose $\theta = 0°$ and slightly larger values of the Reynolds and capillary numbers, $Re = 26$, $\hat{Ca} = 108$, and $Ka = 0.0013$ to test the parameter range.

Variations of the surface profiles corresponding to variations of the flow rate q_0 are shown in Fig. 7. The observed trend is expected, that is the jump region moves away from the entry point with increasing flux rate, that is, with increasing the Reynolds number.

One can also observe the effect of the far-field conditions by changing the size of the flow domain but keeping all other parameters fixed, as is demonstrated in Fig. 8, inset. The larger domains provide stronger resistance to the flow so that the jump regions move closer to the entry point. It is worth noting that the far-field conditions do not affect the upstream profiles, but the transition point. So that the local criteria are indeed insensitive to the far-field conditions contrary to experimental observations.

At the same time, the effect of the capillary numbers in a wide parameter range was very weak and practically negligible, Fig. 8. That is variations of the surface tension over more than a decade do not have any effect on the flow itself and the developing jump region. Also, we have not found so far any capillary-dominant flow regime, as in [23].

These findings are the main results of the study. The observed trends are typical, that is they have been present in the numerical

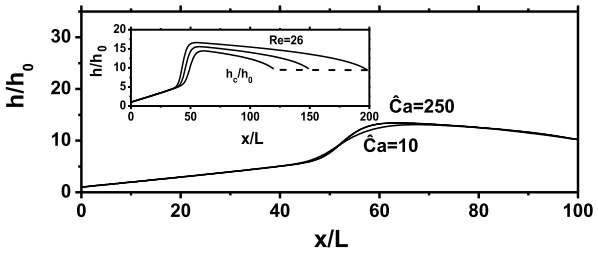

Fig. 8. Free surface profiles calculated numerically at $\theta = 0°$, $Re = 26$ and $Ka = 0.0013$ at different values of $\hat{Ca}$. The insert shows simulations with all parameters fixed at $\theta = 0°$, $Re = 26$, $\hat{Ca} = 108$, $Ka = 0.0013$, but in different domains.

solutions at different parameters within the parameter range in this study.

5. Conclusions

It has been demonstrated that the full DAM possesses continuous, regular solutions manifesting formation of a steady hydraulic jump, and thus continuously linking the two regions, the upstream and the downstream of the flow. A comparison with experimental data has shown that the numerical solution can adequately describe flows with hydraulic jumps in a laminar flow regime, though rather fine resolution of the transition region was required, which might be computationally demanding in case the full Navier-Stokes model would be used.

The obtained numerical solutions demonstrate anticipated trends with variations of the volumetric flux density, and the non-dimensional parameters of the problem. At the same time, the effect of the surface tension was found to be negligible in the formation of a hydraulic jump in the laminar flow regime. This implies that the observed invariance effects [17,18,20–22], which might be initially attributed to the surface tension contribution alone, could be in fact a result of a complex interplay in turbulent flows when, at the same time, the effect of the gravity field was somehow shadowed. Note, the flow turbulisation has been identified as a factor of the jump formation process [3,16,20], but the results imply, fundamentally, that this could be the main factor in the process.

We have observed no transient features present in laminar flow simulations with a hydraulic jump developed using the full system of the Navier-Stokes equations [24,26] and have not identified so far the capillary-dominant laminar flow regime with a hydraulic jump developed.

CRediT authorship contribution statement

Edward Calver: Writing – review & editing, Software, Investigation, Formal analysis. **Tristan Pryer:** Writing – review & editing, Supervision, Software, Methodology, Formal analysis. **Alex V. Lukyanov:** Writing – original draft, Supervision, Conceptualization.

Declaration of competing interest

The authors declare that they have no known competing financial interests or personal relationships that could have appeared to influence the work reported in this paper.

Data availability

The authors do not have permission to share data.

Acknowledgements

The authors are grateful to Prof. D. Ian Wilson and Dr. Rajesh Bhagat for useful discussions. EC was supported through a PhD scholarship awarded by the "EPSRC Centre for Doctoral Training in the Mathematics of Planet Earth at Imperial College London and the University of Reading" EP/L016613/1.

Appendix A. Numerical discretisation and benchmarking

We discretise (9) - (10) through a method of lines approach utilising a finite volume spatial discretisation with a Lax-Friedrichs flux type.

Let $\mathcal{T} = \{x_i\}$ be a partition of the domain $[0, L]$ into cells $K_i = (x_{i-1/2}, x_{i+1/2})$. Here $x_i = \frac{1}{2}(x_{i+1/2} + x_{i-1/2})$ denotes the midpoint of a cell K_i. Let $\Delta x_i = x_{i+1/2} - x_{i-1/2}$ denote the length of the cell. We only consider the case $\Delta x_i \equiv \Delta x$ for all i, however note that various adaptive strategies exist for this class of problems [34] that may be able to provide better resolution at the jump interface.

For exposition, we reformulate (9) - (10) in a conservative form

$$\begin{aligned} \frac{\partial h}{\partial t} + \frac{\partial q}{\partial x} &= 0, \\ \frac{\partial q}{\partial t} + \frac{\partial}{\partial x} F(q,h) - \frac{\partial}{\partial x} G(h) &= -\frac{3}{Re}\frac{q}{h^2}, \end{aligned} \tag{A.1}$$

where

$$\begin{aligned} F(q,h) &= \frac{6}{5}\frac{q^2}{h} - \frac{Ka}{2}h^2 \\ G(h) &= \frac{1}{\hat{Ca}Re}\left(\frac{1}{2}\frac{\partial^2 h^2}{\partial x^2} - \frac{3}{2}\left(\frac{\partial h}{\partial x}\right)^2\right). \end{aligned} \tag{A.2}$$

Let χ_{K_i} denote the indicator function over the cell K_i, we then define our numerical approximation

$$\begin{aligned} H(x,t) &= \sum_i H_i(t)\chi_{K_i}(x) \\ Q(x,t) &= \sum_i Q_i(t)\chi_{K_i}(x), \end{aligned} \tag{A.3}$$

where H_i, Q_i solve the following system of ODEs:

$$\begin{aligned} &\frac{d}{dt}H_i + \frac{1}{\Delta x}\left[Q_{i+1/2} - Q_{i-1/2}\right] = 0 \\ &\frac{d}{dt}Q_i + \frac{1}{\Delta x}\left[\mathcal{F}_{i+1/2} - \mathcal{F}_{i-1/2}\right] + \frac{1}{\Delta x}\left[\mathcal{G}_{i+1/2} - \mathcal{G}_{i-1/2}\right] \\ &\qquad\qquad = -\frac{3}{Re}\frac{Q_i}{H_i^2} \end{aligned} \tag{A.4}$$

and $\mathcal{F}, \mathcal{G}$ represent approximations to F and G respectively.

For our experiments we chose a Lax-Friedrichs flux

$$\begin{aligned} \mathcal{F}_{i+1/2} &= \frac{1}{2}(F(U_i) + F(U_{i+1})) \\ &\quad - \max(\nabla F(U_i), \nabla F(U_{i+1}))\cdot(U_{i+1} - U_i) \\ \mathcal{G}_{i+1/2} &= \frac{W_{i+1} + W_i}{2}, \end{aligned} \tag{A.5}$$

where ∇F is the vector valued gradient of F, $U_i = (Q_i, H_i)$ and W_i represents a standard central approximation to G. This is formally a first order scheme in space, note that higher order schemes are available including MUSCL and WENO schemes.

For the temporal discretisation, we use a third-order strong stability preserving scheme. To ensure the method remains stable we make use of an adaptive time-step chosen to ensure the Courant–Friedrichs–Lewy condition is always met.

To test the method converges we fix parameters $Re = 26$, $\hat{Ca} = 108$, $Ka = 0.0013$ and simulate solutions over a family of mesh sizes until a steady state is found. We select $\Delta x \in [0.00625, 0.05]$ and plot specific numerical profiles in Fig. 4. Notice that the

method is quite diffuse for coarse mesh-scale and the position and profile of the jump is mesh-dependent. To ensure physically accurate results, all our experiments henceforth were obtained using $\Delta x = 0.00625$.

References

[1] Lord Rayleigh, On the theory of long waves and bores, Proc. R. Soc. Lond. A 90 (1914) 324–328.
[2] I. Tani, Water jump in the boundary layer, J. Phys. Soc. Jpn. 4 (1949) 212–215.
[3] E.J. Watson, The radial spread of a liquid jet over a horizontal plane, J. Fluid Mech. 20 (1964) 481–499.
[4] A.D.D. Craik, R.C. Latham, M.J. Fawkes, P.W.F. Gribbon, The circular hydraulic jump, J. Fluid Mech. 112 (1981) 347–362.
[5] T. Bohr, P. Dimon, V. Putkaradze, Shallow-water approach to the circular hydraulic jump, J. Fluid Mech. 254 (1993) 635–648.
[6] X. Liu, J.H. Lienhard, The hydraulic jump in circular jet impingement and in other thin liquid films, Exp. Fluids 15 (1993) 108–116.
[7] F.J. Higuera, The hydraulic jump in a viscous laminar flow, J. Fluid Mech. 274 (1994) 69–92.
[8] F.J. Higuera, The circular hydraulic jump, Phys. Fluids 9 (1997) 1476–1478.
[9] T. Bohr, V. Putkaradze, S. Watanabe, Averaging theory for the structure of hydraulic jumps and separation in laminar free-surface flows, Phys. Rev. Lett. 79 (1997) 1038–1041.
[10] C.T. Avedisian, Z. Zhao, The circular hydraulic jump in low gravity, Proc. R. Soc. Lond. A 456 (2000) 2127–2151.
[11] J.W.M. Bush, J.M. Aristoff, The influence of surface tension on the circular hydraulic jump, J. Fluid Mech. 489 (2003) 229–238.
[12] S.B. Singha, J.K. Bhattacharjee, A.K. Ray, Hydraulic jump in one-dimensional flow, Eur. Phys. J. B 48 (2005) 417–426.
[13] K. Phillips, J.M. Kuhlman, M. Mohebbi, E. Calandrelli, D.D. Gray, Investigation of circular hydraulic jump behavior in microgravity, in: 38th Fluid Dynamics Conference and Exhibit 23 - 26 June 2008, Seattle, Washington, 2008.
[14] R.P. Kate, P.K. Das, S. Chakraborty, An investigation on non-circular hydraulic jumps formed due to obliquely impinging circular liquid jets, Exp. Therm. Fluid Sci. 32 (2008) 1429–1439.
[15] A.R. Kasimov, A stationary circular hydraulic jump, the limits of its existence and its gasdynamic analogue, J. Fluid Mech. 601 (2008) 189–198.
[16] D. Bonn, A. Andersen, T. Bohr, Hydraulic jumps in a channel, J. Fluid Mech. 618 (2009) 71–87.
[17] D.I. Wilson, B.L. Le, H.D.A. Dao, K.Y. Lai, K.R. Morison, J.F. Davidson, Surface flow and drainage films created by horizontal impinging liquid jets, Chem. Eng. Sci. 68 (2012) 449–460.
[18] T. Wang, D. Faria, L.J. Stevens, J.S.C. Tan, J.F. Davidson, D.I. Wilson, Flow patterns and draining films created by horizontal and inclined coherent water jets impinging on vertical walls, Chem. Eng. Sci. 102 (2013) 585–601.
[19] A. Duchesne, L. Lebon, L. Limat, Constant Froude number in a circular hydraulic jump and its implication on the jump radius selection, Europhys. Lett. 107 (2014) 54002.
[20] R.K. Bhagat, D.I. Wilson, Flow in the thin film created by a coherent turbulent water jet impinging on a vertical wall, Chem. Eng. Sci. 152 (2016) 606–623.
[21] R.K. Bhagat, N.K. Jha, P.F. Linden, D.I. Wilson, On the origin of the hydraulic jump in a thin liquid film, arXiv:1712.04255 [physics.flu-dyn], 2017.
[22] R.K. Bhagat, N.K. Jha, P.F. Linden, D.I. Wilson, On the origin of the circular hydraulic jump in a thin liquid film, J. Fluid Mech. 851 (2018) R5.
[23] H. Askarizadeh, H. Ahmadikia, C. Ehrenpreis, R. Kneer, A. Pishevar, W. Rohlfs, Role of gravity and capillary waves in the origin of circular hydraulic jumps, Phys. Rev. Fluids 4 (2019) 114002.
[24] R. Fernandez-Feria, E. Sanmiguel-Rojas, E.S. Benilov, On the origin and structure of a stationary circular hydraulic jump, Phys. Fluids 31 (2019) 072104.
[25] A. Duchesne, A. Andersen, T. Bohr, Surface tension and the origin of the circular hydraulic jump in a thin liquid film, Phys. Rev. Fluids 4 (2019) 084001.
[26] M. Dhar, G. Das, P.K. Das, Planar hydraulic jumps in thin film flow, J. Fluid Mech. 884 (2020) A11.
[27] R.K. Bhagat, P.F. Linden, The circular capillary jump, J. Fluid Mech. 896 (2020) A25.
[28] F. De Vita, P.-Y. Lagrée, S. Chibbaro, S. Popinet, Beyond shallow water: appraisal of a numerical approach to hydraulic jumps based upon the boundary layer theory, Eur. J. Mech. B, Fluids 79 (2020) 233–246.
[29] R.K. Bhagat, D.I. Wilson, P.F. Linden, Experimental evidence for surface tension origin of the circular hydraulic jump, arXiv:2010.04107 [physics.flu-dyn], 2020.
[30] R.K. Bhagat, P.F. Linden, The circular hydraulic jump; the influence of downstream flow on the jump radius, Phys. Fluids 34 (2022) 072111.
[31] A. Duchesne, L. Limat, Circular hydraulic jumps: where does surface tension matter?, J. Fluid Mech. 937 (2022) R2.
[32] F.M. White, Viscous Fluid Flow, McGraw-Hill, 2006.
[33] R.V. Craster, O.K. Matar, Dynamics and stability of thin liquid films, Rev. Mod. Phys. 81 (2009) 1131–1198.
[34] J. Giesselmann, C. Makridakis, T. Pryer, A posteriori analysis of discontinuous Galerkin schemes for systems of hyperbolic conservation laws, SIAM J. Numer. Anal. 53 (2015) 1280–1303.